ENGINEERING Agriculture

Engineering Journals

RESEARCH ARTICLE

2026 / Volume 13 / Issue 4 / 26673

Multidimensional effects and mechanisms of micro-nano bubbles in regulating waterlogged soil microenvironments

Zhihao CHEN[1,2,3,4], Shunyao ZHUANG[1], Yonghong WU (✉)[1,2,4]

1 State Key Laboratory of Soil and Sustainable Agriculture, Institute of Soil Science, Chinese Academy of Sciences, Nanjing 211135, China.
2 Zigui Three Gorges Reservoir Ecosystem, Observation and Research Station of Ministry of Water Resources of the People's Republic of China, Yichang 443605, China.
3 University of Chinese Academy of Sciences (Beijing), Beijing 100049, China.
4 University of Chinese Academy of Sciences, Nanjing, Nanjing 211135, China.

KEYWORDS

Micro-nano bubbles, nutrient use efficiency, soil ecology, soil remediation, waterlogged soil

HIGHLIGHTS

- Micro-nano bubbles significantly increase soil micropores and oxidation-reduction potential (ORP).
- Pore structure and ORP synergistically regulate nutrient availability.
- Increased genes involved in C, N and P cycling (CNP genes) abundance enhances nutrient transformation and reduces global warming potential.
- Micropore structure is likely to contribute to waterlogged soil functions.
- Micro-nano bubble treatment is expected to promote efficient agricultural production.

Received October 9, 2025;
Accepted November 7, 2025.

Correspondence: yhwu@issas.ac.cn

GRAPHICAL ABSTRACT

ABSTRACT

Prolonged flooding creates strongly reductive paddy soils that limit nutrient availability and increase greenhouse gas emissions. To address this issue, air and oxygen micro-nano bubbles were evaluated as a low-input amendment in a pot experiment. The oxygen bubbles remodeled soil structure (increased micropores 2.4 times) and raised soil ORP to 374 mV. These changes expanded the abundances of CNP genes, reduced total reducing substances by 22.4%, improved nutrient availability (increased alkali-hydrolyzable nitrogen, available phosphorus and potassium to 216, 72.2 and 284 mg·kg^{-1}, respectively), and lowered the global warming potential by about 26%. Correlation and path

analyses indicated that micropore expansion, rather than greater connectivity, plus moderate re-oxidation drove microbial functional gains, nutrient release and methane oxidation. This study offers valuable insights into the multidimensional connection of soil structure, nutrients and soil ecology and it offers a chemical-free route for the green remediation of waterlogged fields.

1 Introduction

Food security remains a global challenge amid population growth and shrinking arable land. The UN Food and Agriculture Organization predicts that global food production must increase by 45% by 2050 (relative to 2010) to meet demand[1,2]. However, low-yield fields (e.g., waterlogged paddies, saline-alkali soils and acidified soils) severely constrain agricultural productivity[3]. Waterlogged paddies, characterized by persistent inundation and reductive conditions, are widespread in southern China and other rain-rich, low-lying regions[4]. These fields account for 15%–20% of total rice area in these regions, with yields typically 30%–50% lower than normal paddies, often leading to soil gleization[5,6]. Due to waterlogging and strong reduction, concentrations of Fe^{2+}, Mn^{2+} and organic acids rise, directly poisoning rice roots and causing seedling stunting and black root disease[7–9]. Additionally, phosphorus is immobilized by ferrous ions into insoluble Fe-P, decreasing its availability[10] and exacerbating vulnerabilities in food production.

Ecological impacts are also substantial but often overlooked. Flooded rice fields are the largest agricultural source of methane emissions, contributing 10%–15% of global anthropogenic emissions[11]. Prolonged anoxia in waterlogged soils stimulates methanogens (e.g., *Methanosarcina*), increasing CH_4 emissions 1.5–2 times above normal paddies[12,13]. Similarly, nitrification is inhibited while denitrification may be enhanced, potentially boosting nitrous oxide emissions[14,15]. Weak nutrient retention in waterlogged soils also promotes N and P losses via drainage, worsening non-point source pollution[7]. Also, the soil microbial community shifts toward anaerobe dominance, suppressing aerobic microbes involved in organic matter decomposition and nutrient cycling[16], impairing microecological health.

The detrimental effects of waterlogged paddies are multidimensional, encompassing both food production and ecological concerns. Remediation is therefore critical. Standard remediation, engineering drainage, chemical amendments and biological measures, has limitations. Engineering drainage (ditches and subsurface pipes) lowers the water table and improves soil aeration[17,18], but is expensive, maintenance-intensive and prone to nutrient leaching. Waterlogging-prone fields often occur in areas with inherently high water tables and rainfall, making environmental changes difficult[19]. Chemical amendments, such as lime or calcium peroxide, can raise soil ORP[20,21], but may not be sustainable and can disrupt pH balance. Biological approaches (waterlogging-tolerant crops and organic fertilizers)[22] are ecofriendly but slow-acting. These shortcomings motivate greener, more robust solutions.

Micro-nano bubble (MNB) technology offers a potential new solution. MNBs, also known as ultrafine bubbles, are nanoscopic gaseous domains than can exist on solid surfaces or in bulk liquids, which are generated by shearing air or oxygen into micron/nanometer sizes, or directly in water via electrolysis[23]. These bubbles with long residence times and high gas dissolution can generate reactive oxygen species[24]. Due to operational flexibility, environmental friendliness and near-zero operating costs, MNBs have been applied in wastewater treatment, soil remediation[25] and greenhouse gas emission reduction. For example, MNB ozonation removed over 99% of ibuprofen (~50 mg·L^{-1}) in 70 min[26], decreased the pH of saline-alkali soil by 5%[27] and increased CH_4 uptake by about threefold[28]. These applications primarily leverage oxidative capacity of the MNBs to degrade pollutants and stimulate aerobic microbial activity[29]. However, the effectiveness of MNBs in strongly reductive waterlogged paddy soils has not been examined.

We hypothesized that MNBs would (1) act as microscopic oxygen pumps, gradually releasing oxygen to elevate soil ORP and mitigate strong reduction, (2) improve the soil microenvironment to cut greenhouse gas emissions and enhance microbial health, and (3) directly remodel the

micropore system to facilitate oxygen diffusion and fundamentally change adverse soil conditions. To test this, we investigated whether air and O_2 MNBs could improve soil function and ecological health in waterlogged paddies, elucidating the underlying physical-chemical-microbial mechanisms. The aim is to provide a low-cost solution for managing waterlogged low-yield fields and promoting green, efficient agriculture, as well as to gain insights into how soil microstructure, nutrients and microbes collectively influence soil function and ecology under flooding.

2 Materials and methods

2.1 Soil collection

Soil was collected in early April from a flooded rice paddy near Wusha Town, Chizhou City, Anhui Province, China (30°34′21″ N, 117°17′38″ E) prior to sowing. The site lies on the transitional zone between the Yangtze River floodplain and southern Anhui hills, characterized by a subtropical humid monsoon climate with distinct seasons and abundant annual rainfall (average 1600 mm). The area has dense water networks near the Qiupu and Jiuhua rivers and typically supports single- or double-cropping rice, making it a key rice-producing region in southern Anhui.

Soils in Wusha Town are mainly clay loam or silty clay, with strong water retention (Table 1) but poor aeration, prone to plow pan formation. Seasonal waterlogging, high groundwater tables and long-term flooded cultivation contribute to widespread waterlogging issues.

Table 1 Physical and chemical properties of the experimental paddy soil in Wusha Town

Property	Value
Water content (%)	59.2 ± 3.6
pH	4.58 ± 0.01
Oxidation-reduction potential	222 ± 1.9
Saturated water content ($g \cdot kg^{-1}$)	621 ± 17.6
Clay ratio (%)	26.0 ± 0.6
Soil organic C ($g \cdot kg^{-1}$)	18.7 ± 0.1
Total N ($g \cdot kg^{-1}$)	1.71 ± 0.03
Fe^{2+} ($cmol \cdot kg^{-1}$)	1.1 ± 0.1
Total reducing substances ($cmol \cdot kg^{-1}$)	9.5 ± 0.2
Alkali-hydrolyzable N ($mg \cdot kg^{-1}$)	174 ± 3.2
Available P ($mg \cdot kg^{-1}$)	23.0 ± 0.9
Available K ($mg \cdot kg^{-1}$)	111 ± 7.7

2.2 Experimental design

A pot experiment was conducted from April to May 2025. Topsoil (5–20 cm depth) was collected, roots removed and packed into pots (Ø 20 cm × 25 cm). A constant 5-cm water layer was maintained for 1 week for stabilization before MNB treatment. Two types of MNBs, air and O_2, were generated using a micro-nano bubbles generator (150 $L \cdot h^{-1}$, Yuchuang Environmental Technology Co., Ltd.). Specifically, the generator sheared the supplied air or O_2 into a large number of ultrafine bubbles and pumped them into the water, thereby creating air- or O_2-treated water, which was then used for irrigation. Bubble size distributions are given in Table S1.

Three treatments were applied: an untreated control (CK), Air-MNBs (aerated with air-MNBs) and O_2-MNBs (aerated with O_2-MNBs). Each treatment had three replicates with all pots maintained > 3 cm of overlying water and the overlying water treated every 4 days. In total the treatments were applied 10 times on Days 0, 4, 8, 12, 16, 20, 24, 28, 32 and 36. During the course of the experiment, evaporated water was replenished to maintain waterlogged. The experiment ended on Day 40 for sampling and analyses.

2.3 Sample collection and analyses

Fresh soil weight (m_1) was recorded, oven-dried at 105 °C to constant weight (m_2), and water content (w) calculated as:

$$w = \frac{m_1 - m_2}{m_2} \times 100\% \quad (1)$$

Soil was mixed with ultrapure water (2.5:1 v/w), settled and supernatant pH was measured with a pH meter. Soil ORP was measured in situ using an ORP meter (TR-901, Shanghai Leici Co., Ltd., Shanghai, China). Saturated water content was determined through a 100-cm^3 ring knife[30]. The particle size distribution of soil and bubble size distribution of MNBs were analyzed using a Mastersizer 3000 analyzer (Malvern Panalytical, Almelo, Netherlands)[31].

Fresh soil extracted with 2 $mol \cdot L^{-1}$ KCl (5:1 v/w). Filtrate (< 0.22 μm) was analyzed for soil ammonium N (NH_4^+-N) and

nitrate N (NO_3^--N) by a continuous-flow autoanalyzer (AA3, Seal Analytical GmbH, Norderstedt, Germany)[32]. Results were converted to dry weight basis. Soil (air-dried) organic carbon (SOC) and total nitrogen (TN) was measured by elemental analyzer (Vario TOC, Elementar Analysensysteme GmbH, Langenselbold, Germany)[33]. Fresh soil was extracted with 0.1 mol·L^{-1} $Al_2(SO_4)_3$ (pH 2.50, 20:1 v/w), allowed to settled and filtered by filter paper. The filtrate was analyzed for total reducing substances (TRS) and active reducing substances (ARS) via oxidation with $K_2Cr_2O_7$ and $KMnO_4$, followed by titration, respectively. Fe^{2+} was determined by o-phenanthroline colorimetry[4]. Results were converted to dry weight basis. Alkali-hydrolyzable N (AN), available P (AP) and available K (AK) were determined by alkali diffusion, $NaHCO_3$ extraction-molybdenum blue spectrophotometry and cold HNO_3 extraction-flame photometry, respectively[34].

Small plexiglass static chambers were placed over pots to collected gas samples, then the concentrations of CO_2, CH_4 and N_2O were measured by gas chromatography (7890B, Agilent, Santa Clara, CA, USA). Emission fluxes were calculated based on chamber volume.

Intact soil cores were collected by PVC pipes (Ø 2.2 cm × 4 cm) and scanned using micro-CT (XploreVista 2000 4D, Microcant Technology (Suzhou) Co., Ltd., Suzhou, Jiangsu, China) under 100 kV and 110 μA to quantify pore distribution[35]. The voxel resolution was about 25 μm. For image segmentation, the boundaries were refined using the Interactive Thresholding module in Avizo and 3D connectivity analysis was performed using the Segmentation module. The pores were divided into four classes: micropores (< 100 μm), mesopores (100–200 μm), macropores (200–500 μm) and ultra-macropores (> 500 μm).

Samples used for microorganism and gene analyses were stored at −80 °C until DNA extraction. Total DNA was extracted using FastDNA SPIN Kit for soil (MP Biomedicals, Irvine, CA, USA) following the manufacturer's instructions. DNA concentration and quality were assessed by a spectrophotometer (NanoDrop ND-8000, Thermo Fisher Scientific, Waltham, MA, USA) and 1.5% agarose gel electrophoresis. The extracted DNA was stored at −80 °C for amplification and sequencing.

16S rRNA gene V3-V4 regions were amplified. Primers used were 338F (5′-ACTCCTACGGGAGGCAGCAG-3′) and 806R (5′-GGACTACHVGGGTWTCTAAT-3′)[36]. Sequencing was performed on an NovaSeq 6000 (Illumina, San Diego, CA, USA). Raw reads were filtered by Trimmomatic v0.33[37]. Primer identification and removal were done by Cutadapt v1.9.1[38]. Denoising and chimera removal were done in QIIME2[39] by dada2[40]. Finally, the species classification was carried out according to the SILVA database[41].

High-throughput quantitative PCR (HT-qPCR) of CNP genes (Table S2) were performed using a WaferGen SmartChip Real-Time PCR System (Hefei Yuanzai Biotechnology Co., Ltd., Hefei, Anhui, China). A 72-primer by 72-sample array was used to load the samples on SmartChip Multisample Nanodispenser (Hefei Yuanzai Biotechnology Co.). Reactions were conducted in 100 nL comprising 50 nL 2 × LightCycler 480 SYBR Green I Master Mix (Roche Inc., Indianapolis, IN, USA), 20 nL DNA template (2 ng·μL^{-1}), 1 nL bovine serum albumin (0.1 mg·L^{-1}), 5 nL forward primers, 5 nL reverse primers and 19 nL nuclease-free water. Amplification was performed with three repeats, including a non-template control. Amplification conditions were: initial denaturation at 94 °C for 2 min; followed by 40 cycles of 94 °C for 30 s (denaturation), 52 °C for 30 s (annealing) and 72 °C for 30 s (extension); finally, generate a melting curve automatically by the instrument[42]. The results of HT-qPCR were analyzed using SmartChip qPCR software, and positive amplification was defined as Ct < 31 cycles and more than two repeated amplification. Then gene copy numbers were calculated.

2.4 Data analyses

Figures were created using Origin 9.0. Statistical analyses were performed. One-way ANOVA and Spearman correlation were conducted using SPSS 17.0 software. α-Diversity differences between microbial groups were assessed by the Kruskal–Wallis test. Permutational multivariate analysis of variance was used to confirm whether the difference of β-diversity between groups was significant. Non-metric multidimensional scaling (NMDS) visualized microbial community differences. Unless otherwise specified, the analyses of microbial community and diversity was conducted at the genus level based on Bray-Curtis distance[43]. Partial least squares path modeling (PLS-PM) analysis was performed using the R package "plspm"[44]. The significance level was set at $P < 0.05$ for all analyses.

3 Results

3.1 Soil pore network

The CT scan quantified pore distribution and revealed that the MNB treatments significantly altered soil pore structure. As given in Tables S3 and S4, the volume proportion and porosity of micropores (< 100 μm), mesopores (100–200 μm) were increased. Compared to CK, Air-MNBs increased micropore volume proportion by 1.3 times ($P > 0.05$) and O_2-MNBs increased micropore volume proportion by 2.4 times ($P < 0.05$). Meanwhile, micropore porosity increased by 1.4 times (Air-MNBs, $P > 0.05$) and 3.0 times (O_2-MNBs, $P < 0.05$). Similarly, mesopore volume proportion increased from 2.28% (CK) to 4.55% (Air-MNBs, $P > 0.05$) and 6.15% (O_2-MNBs, $P > 0.05$), and mesopore porosity increased from 0.10% (CK) to 0.22% (Air-MNBs, $P > 0.05$) and 0.34% (O_2-MNBs, $P > 0.05$). Macropore (200–500 μm) volume increases were not significant. Ultra-macropore (> 500 μm) volume proportion decreased (CK 90.7%; Air-MNBs 84.3%, $P > 0.05$; and O_2-MNBs 80.5%, $P < 0.05$). Ultra-macropore porosity remained unchanged.

Micropores, mesopores and macropores contributed < 20% to total pore volume percentage (Table S3). However, they possess large specific surface areas (SSA), which are likely to contribute to soil structure and functions. As shown in Fig. S1(a), soil SSA in CK was 748 m^{-1}, and increased to 1050 m^{-1} ($P > 0.05$) and 1410 m^{-1} ($P < 0.05$) with Air- and O_2-MNBs, respectively. Visually, MNB-treated soils had denser pore networks (Fig. S1(b–d)).

However, MNBs did not significantly improve pore connectivity (Fig. S2(a)), a finding consistent with 3D images of connected pores (Fig. S2(b–d)), where MNB-treated connected pores showed no increased complexity compared to CK. Also, quantitative throat analysis did not reveal any significant changes in connected pore throats. Figure 1(a–c) (ball-and-stick models of pores and throats) indicate more pores and throats in MNB-treated soils, but further analysis revealed that coordination number significantly decreased. Coordination number is the average connections per pore, and decreased by > 60% with MNB treatment (0.44 in Air-MNBs and 0.27 in O_2-MNBs) (Fig. 1(d)). While pore-to-throat number ratios increased from 1.93 to 4.69 (Air-MNBs, $P > 0.05$) and 7.88 (O_2-MNBs, $P < 0.05$) (Fig. 1(e)). This increase likely occurred because throat number increased less than pore number. Additionally, increased micropores and mesopores reduced the average equivalent radius of pores (data not shown), but the average throat radius remained unchanged (Fig. 1(f)), leading to significant decreases in average pore-to-throat diameter ratios by 46.9% and 62.2% (Fig. 1(g)). No significant differences were observed in average throat length (Fig. 1(h)) or area (Fig. 1(i)) between treatments.

3.2 Soil reductive status and nutrient availability

To assess chemical improvements from MNB treatments, changes in soil reductive status and nutrient availability were analyzed. ORP reached 374 mV in O_2-MNBs, a 62.6% increase from 230 mV in CK ($P < 0.05$, Fig. S3(b)). Air-MNBs also gave a 51.4% increase in ORP ($P < 0.05$, Fig. S3(b)). Correspondingly, reducing substances decreased significantly. TRS in Air- and O_2-MNBs were 19.3% ($P < 0.05$) and 22.4% ($P < 0.05$) lower than CK (Fig. 2(a)), respectively, and Fe^{2+} contents decreased by 38.5% ($P < 0.05$) and 53.2% ($P < 0.05$) (Fig. 2(c)), respectively. However, ARS did not change significantly (Fig. 2(b)), but active organic reducing substances increased significantly (Fig. 2(d)). Soil pH remained unchanged (Fig. S3(a)).

MNB treatment positively affected nutrient availability. AN increased by 10.3% (Air-MNBs, $P > 0.05$) and 24.4% (O_2-MNBs, $P < 0.05$) compared to CK (Fig. 3(b)), indicating enhanced organic nitrogen mineralization. However, inorganic nitrogen (NH_4^+-N and NO_3^--N) was stable (Fig. 3(c,d)). O_2-MNBs increased AP from 35.6 to 72.2 $mg \cdot kg^{-1}$ ($P < 0.05$, Fig. S4(a)) and AK from 163 to 284 $mg \cdot kg^{-1}$ ($P < 0.05$, Fig. S4(b)). Air-MNBs also increased AP and AK by 33.1% ($P > 0.05$) and 35.9% ($P > 0.05$), respectively, but to a lesser extent than O_2-MNBs.

3.3 Greenhouse gas emissions

Figure 4 shows the effects of MNB treatment on greenhouse gas emissions. O_2-MNBs increased CO_2 flux from 52.6 to 116 $mg \cdot m^{-2} \cdot h^{-1}$ ($P < 0.05$, Fig. 4(a)), more than doubling emissions. CH_4 flux decreased in Air- and O_2-MNBs by 32.6% ($P < 0.05$) and 60.6% ($P < 0.05$) (Fig. 4(b)). For N_2O flux, there were no significant differences or clear trends between treatments (Fig. 4(c)). Global warming potential (GWP) was calculated to integrate CH_4, N_2O and CO_2 emissions. GWP decreased by 15.8% (Air-MNBs, $P > 0.05$) and 26.2% (O_2-MNBs, $P < 0.05$) compared to CK (Fig. 4(d)). Thus, O_2-MNBs significantly reduced overall greenhouse gas emissions.

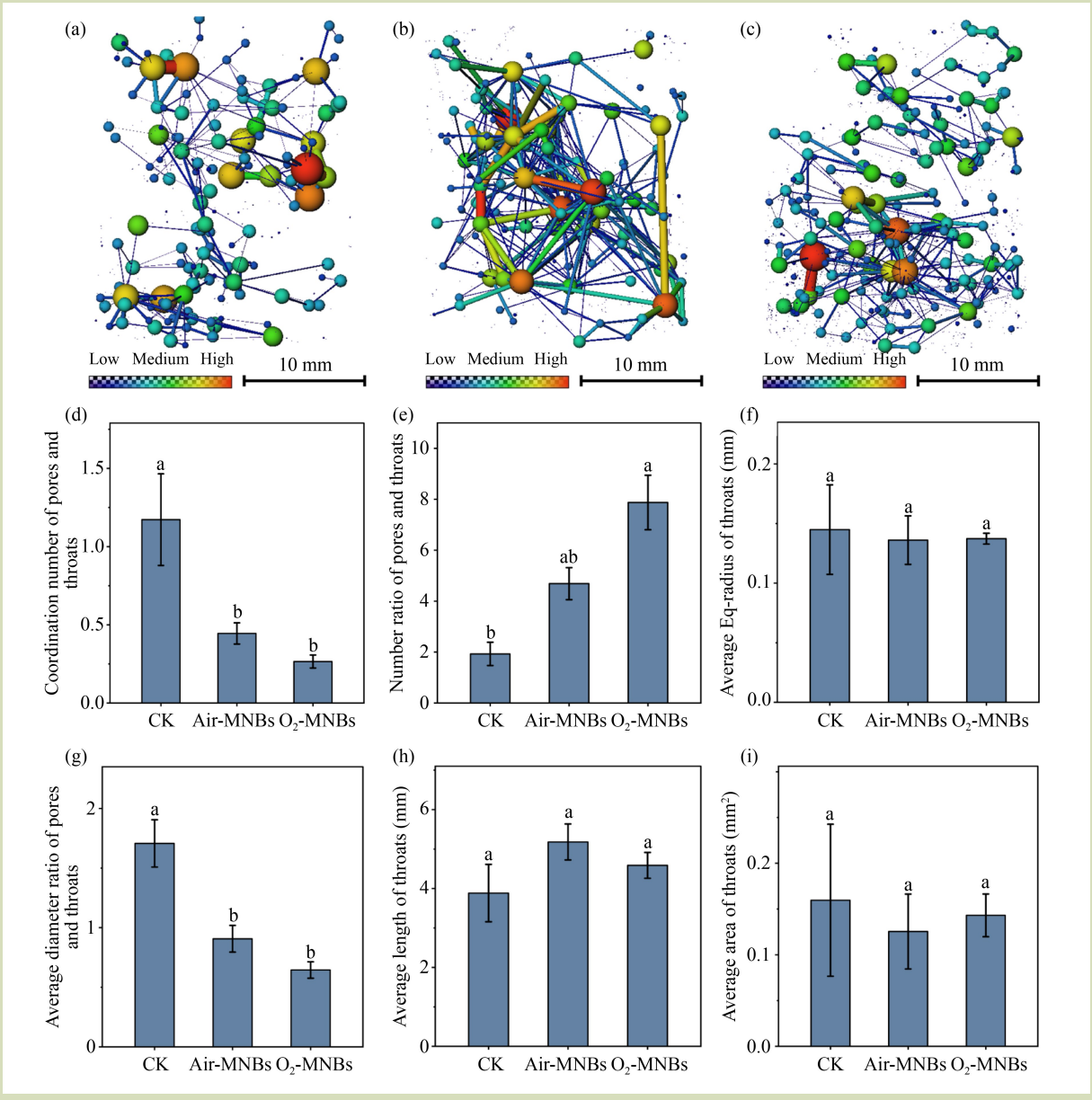

Fig. 1 Pore and throat properties of the soil. Ball-and-stick models of soil pores and throats in the treatments (a) CK, (b) air- and (c) O_2-MNBs. The balls represent pores and the color bar from blue to red represents the pore diameter from small to large. The sticks represent throats and their thickness represents throat diameter. (d) Coordination number of pores and throats, which is the statistical average of the number of throats connected by a single pore; (e) number ratio of pores and throats; (f) average Eq-radius of throats; (g) average diameter ratio of pores and throats; (h) average length of throats; and (i) average area of throats.

3.4 Microorganisms and functional genes

To further explore microbial responses to MNB treatment, microbial community (phylum and genus levels) and absolute abundances of CNP genes were analyzed. No significant differences in α-diversity indices (Shannon, Simpson, ACE and Chao1) were observed between treatments (Table S5). At the genus level, 71% of genera were shared across treatments (Fig. S5(a)), and less than 10% of genera unique to CK

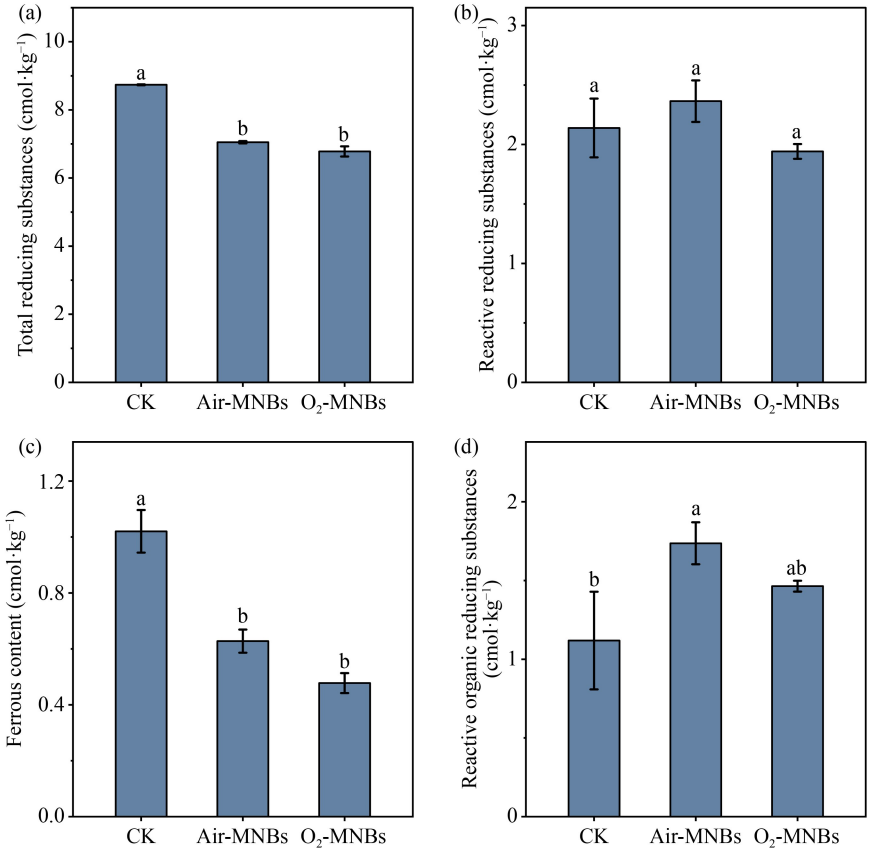

Fig. 2 Reducing substances content of the soil. (a) Total reducing substances; (b) reactive reducing substances; (c) Fe^{2+} content; and (d) reactive organic reducing substances.

disappeared after MNB treatments. Average variation degree (microbial community stability) was nearly identical between groups (Fig. S5(b)). Dominant phyla/genera persisted, but relative abundances shifted. For example, Pseudomonadota and Thermodesulfobacteriota increased, while Chloroflexota and Acidobacteriota decreased after MNB treatments (Fig. S5(c)).

NMDS analysis clearly showed significant separation of microbial communities between treatments (stress = 0.031, P = 0.016, Fig. S6(a)), confirming structural changes. The genera with significant abundance changes were: an unranked Thermodesulfovibrionia increased from 3.6% in CK to 4.5% (Air-MNBs) and 4.2% (O_2-MNBs); an unranked Anaerolineaceae decreased from 5.8% to 3.5% and 2.8%; and genera with ~1% abundance (e.g., an unranked taxa RBG-13-54-9, an unranked Haliangiaceae and *Anaerolinea*) were also affected (Fig. S6(b)). Microbial network analysis showed denser genus-level associations in O_2-MNBs (Fig. S7(c)). Topological analysis revealed O_2-MNBs increased total links (481 vs 408 in CK), with a 15% higher average degree (Table S6). This means closer microbial interactions, but this was not seen in Air-MNBs.

Functional gene quantification showed significantly increased absolute abundances of CNP genes in MNB-treated soils (Fig. 5(a)). C degradation genes in O_2-MNBs increased significantly (Fig. 5(b)), particularly genes for metabolizing recalcitrant organics (lignin and pectin), with > 90% increases, indicating enhanced organics decomposition and accelerated C cycling. Methane oxidation gene abundance increased by 77% in O_2-MNBs (P < 0.05, Fig. 5(c)), reflecting enhanced methanotroph activity and CH_4 oxidation capacity. N transformation genes generally increased, but unexpectedly,

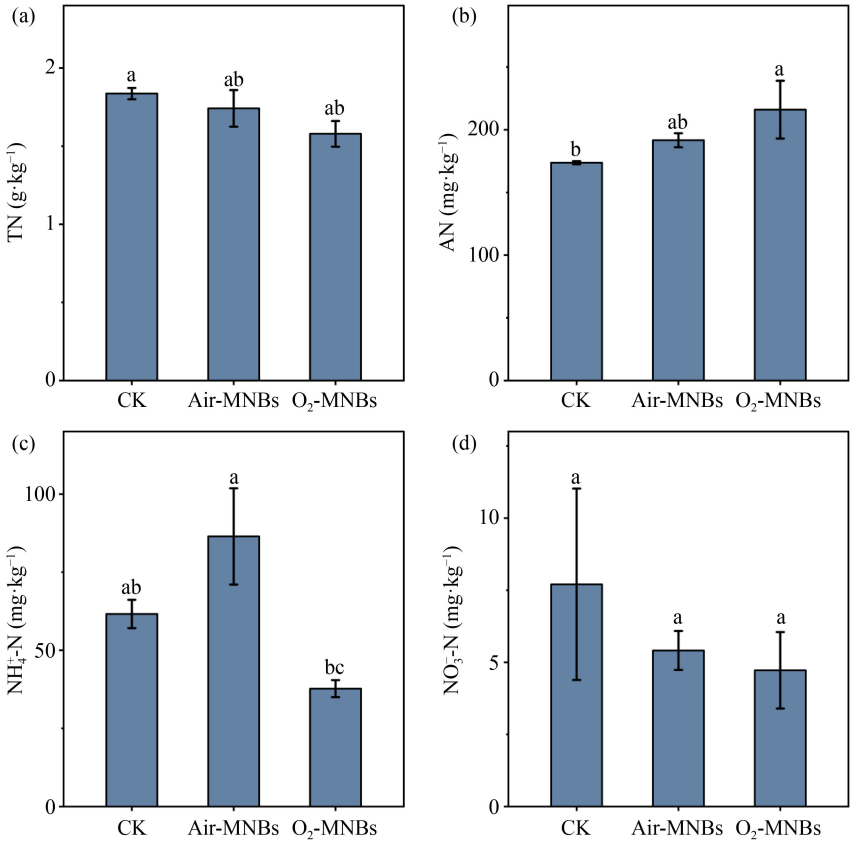

Fig. 3 Nitrogen content of the soil. (a) Total N (TN); (b) alkali-hydrolyzable N (AN); (c) ammonium N (NH_4^+-N); and (d) nitrate N (NO_3^--N).

ammonification (*ureC*) and ammonia oxidation genes (*amoA-1*, *amoA-2*, *amoB* and *hao*) had no significant changes (Fig. 5(d)). While denitrification and N fixation genes (anaerobic metabolism) increased significantly. Additionally, organic P mineralization genes (*phoD*, *phoX*, *bpp* and *cphy*) and solubilization (*gcd* and *pqqC*) genes increased by 72% and 71% in O_2-MNBs ($P < 0.05$, Fig. 5(e)). These increases aligned with increased AP, indicating enhanced microbial P mineralization and solubilization. Air-MNBs gave weaker positive effects on gene abundance.

3.5 Correlation analyses

MNB treatments directly altered soil pore structure and ORP, thus, correlations with reductive species, nutrients, microbial genes and greenhouse gas emissions were analyzed. Figure 6 (significant correlations only) indicates interconnections between pore structure indicators. Generally, more micropores correlated with SSA, smaller diameter ratio of pores and throats (diameter ratio), larger number ratio of pores and throats (number ratio), and lower coordination number of pores and throats (coordination number). Spearman correlation confirmed significant negative correlations of coordination number and diameter ratio with micropore and mesopore porosity, and positive correlations of SSA and number ratio with micropore and mesopore porosity. Micropore porosity had a negative correlation with TRS ($r = -0.97$, $P < 0.001$) and Fe^{2+} ($r = -0.93$, $P < 0.001$) had positive correlations with AN, AP, AK and genes involved in the abundances of CNP genes ($r = 0.72$–0.93, $P = 0.001$–0.037), and a negative correlation with GWP ($r = -0.78$, $P = 0.017$). Similarly, higher ORP correlated with lower TRS ($r = -0.99$, $P < 0.001$), Fe^{2+} ($r = -0.93$, $P < 0.001$) and GWP ($r = -0.85$, $P = 0.006$), and higher AN, AP, AK and gene abundances ($r = 0.83$–0.97, $P < 0.01$).

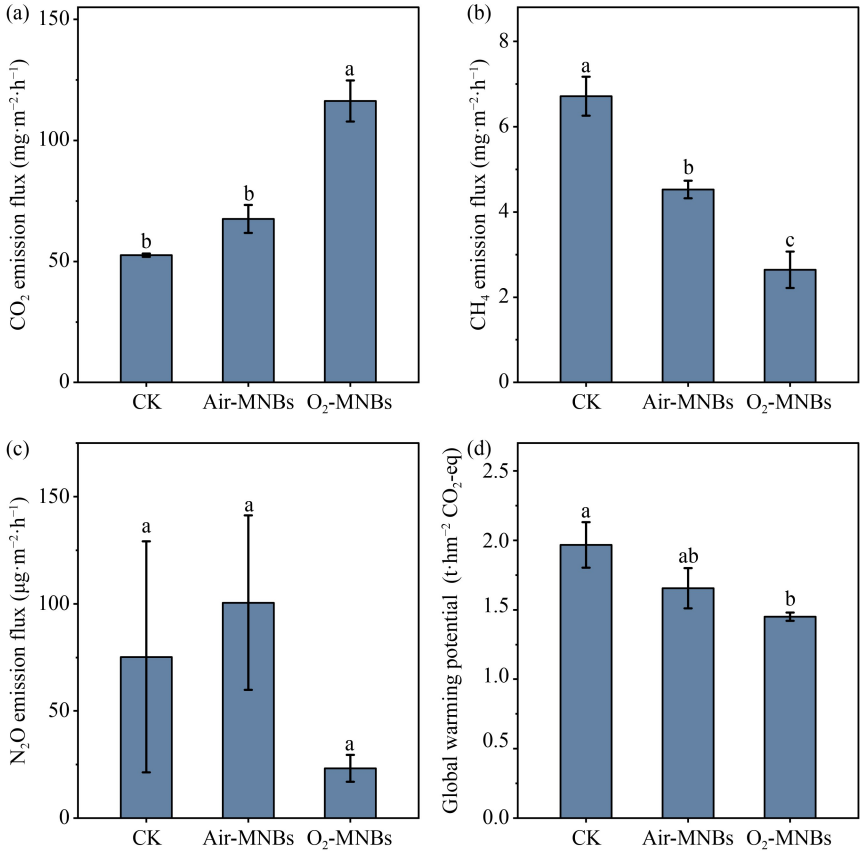

Fig. 4 Greenhouse gas emission fluxes. (a) CO_2 emission flux; (b) CH_4 emission flux; (c) N_2O emission flux; and (d) global warming potential.

Mantel tests analyzed overall effects of pore structure and ORP on other indicators (Fig. S8). Reducing substances (TRS and Fe^{2+}) were correlated with all pore metrics (r = 0.52–0.82, P = 0.001–0.008), but more strongly with ORP (r = 0.99, P = 0.002). Soil nutrients (NPK) correlated with ORP (r = 0.46, P = 0.015) but more strongly with most pore metrics (r = 0.70–0.77, P = 0.001–0.003); the exceptions were coordination number and diameter ratio. This indicates micropore volume (not connectivity) primarily affects nutrient availability. Similarly, greenhouse gas fluxes correlated significantly with all pore metrics (r = 0.53–0.71, P = 0.002–0.012). This correlation was stronger than with ORP (r = 0.45, P = 0.023), further highlighting the importance of pore structure.

PLS-PM was used to examine integrated mechanisms. Significant positive effects of soil structure on soil nutrients (path coefficient 0.933) and ecology (path coefficient 0.663) were observed (Fig. S9(a)). Nutrients did not significantly affect ecology. No direct effect of ORP on ecology but a significant positive effect on nutrients (path coefficient 0.897) were observed (Fig. S9(b)), which in turn affected ecology (path coefficient 0.586). Thus, soil structure and ORP influence nutrients and ecology in different ways. Limitations in sample size prevented constructing PLS-PM with more than three variables to fully resolve joint effects, a focus for future work.

4 Discussion

4.1 Mechanisms of micro-nano bubble-induced soil structure remodeling

Soil pore networks enable matter cycling and microbial activity and influence aeration, water retention and nutrient transformation[46]. O_2-MNBs increased micropores 2.4 times and nearly doubling SSA. This highlights precise regulation of

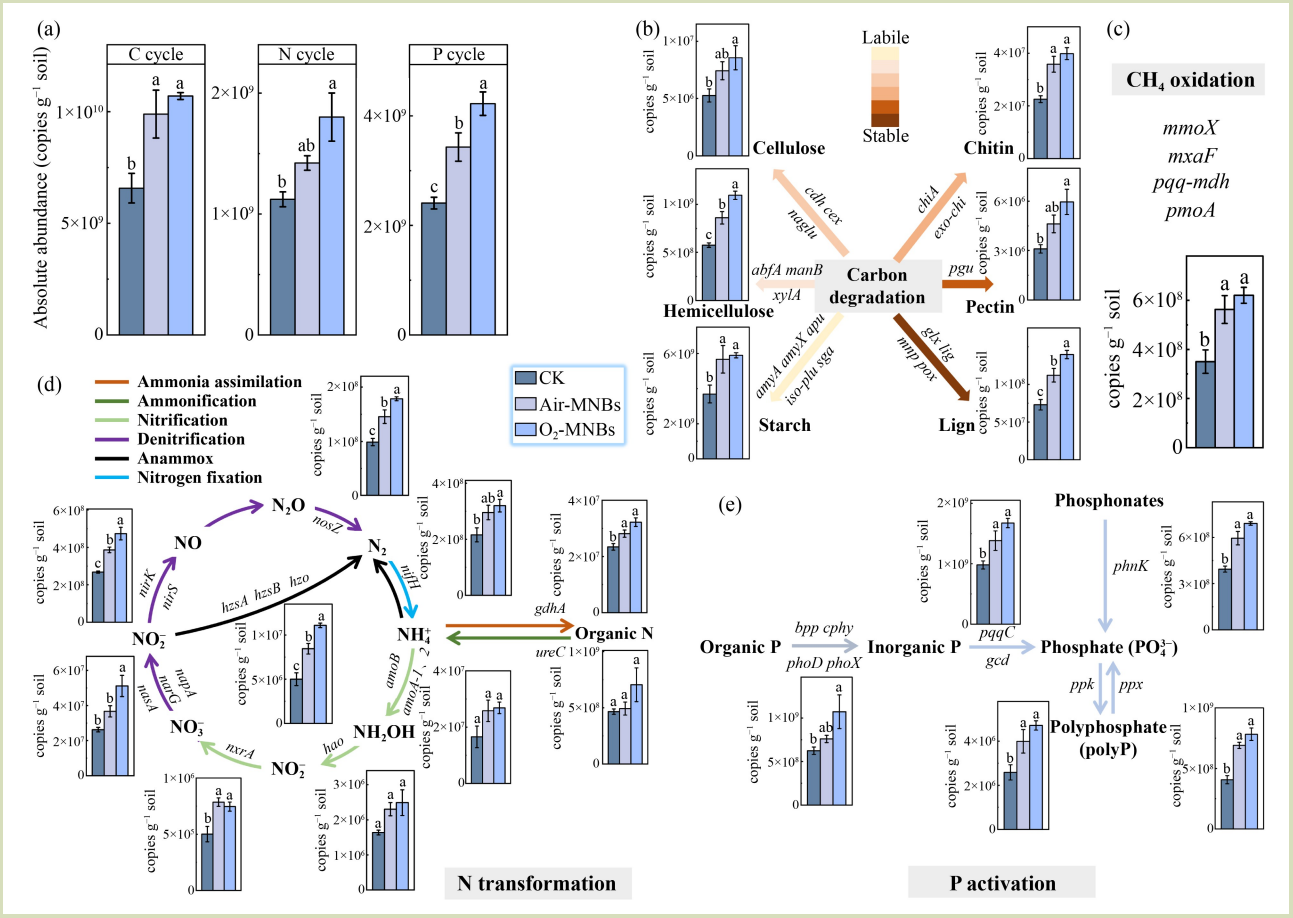

Fig. 5 Microbial gene abundances for C, N and P cycling in the soil. (a) Sum of absolute abundances of all the genes involved in C, N and P cycling measured by the qPCR; and absolute abundances of microbial genes participated in the typical pathways of (b) carbon degradation (genes *amyA*, *amyX*, *apu*, *iso-plu*, *sga*, *abfA*, *manB*, *xylA*, *cdh*, *cex*, *naglu*, *chiA*, *exo-chi*, *pgu*, *glx*, *lig*, *mnp* and *pox*), (c) methane oxidation (genes *mmoX*, *mxaF*, *pqq-mdh* and *pmoA*), (d) inorganic N transformation (genes *gdhA*, *ureC*, *amoA-1*, *amoA-2*, *amoB*, *hao*, *nxrA*, *napA*, *narG*, *nasA*, *nirK-1*, *nirK-2*, *nirK-3*, *nirS-1*, *nirS-2*, *nirS-3*, *hzsA*, *hzsB*, *hzo*, *nosZ-1*, *nosZ-2* and *nifH*), and (e) P solubilization (genes *bpp*, *cphy*, *phoD*, *phoX*, *phnK*, *pqqC*, *gcd*, *ppk* and *ppx*)[45].

soil microstructure by MNBs, contrasting with standard engineering drainage, which primarily alters macropores[47].

The small size (micro to nano scale) of MNBs is key. As MNBs rise and collapse, microscale hydraulic disturbances occur. These disturbances may disperse soil aggregates, forming more micropores[48]. Additionally, bubble surface charge (Zeta potential) may alter electrostatic forces between soil particles[49]. This alteration reduces clay aggregation and further increases micropores.

Crucially, MNBs increased micropores and mesopores without improving connectivity. Coordination number dropped by > 60% due to more micropores. Thus, MNBs tended to form isolated micro-channels rather than continuous macropore networks. This has dual ecological implications. First, increased SSA provides more sites for microbial colonization and nutrient adsorption[50,51]. This matches the positive correlations between micropore porosity and gene abundance. Second, modest connectivity (not increased) may slow O_2 diffusion[52] and then prolong its action. It prevents abrupt redox fluctuations, stabilizing microenvironment for microorganisms. This offers new insights into physical structure-function coupling in waterlogged soils, specifically,

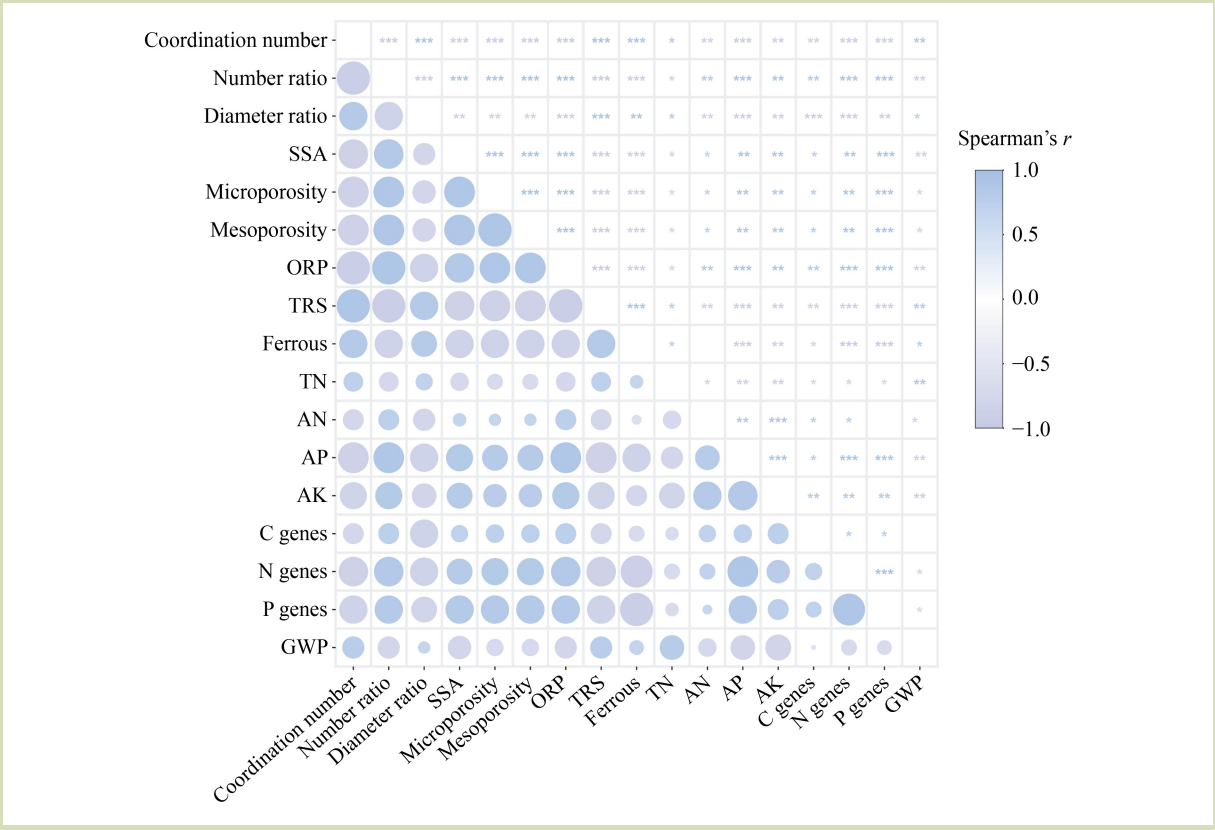

Fig. 6 Spearman correlations between soil pores, environmental factors, functional genes and greenhouse gas emissions. * $P < 0.05$, ** $P < 0.01$ and *** $P < 0.001$. Coordination number is for pores and throats, which is the statistical average of the number of throats connected by a single pore; number ratio is for pores and throats; diameter ratio is the average diameter ratio of pores and throats; SSA is the specific surface area of soil pores; microporosity is the micropore porosity, porosity of pores with diameter < 100 μm; mesoporosity is the mesopore porosity, porosity of pores with diameter 100–200 μm; ORP, oxidation-reduction potential; TRS, total reducing substances; Ferrous, Fe^{2+} content; TN, total nitrogen; AN, alkali-hydrolyzable N; AP, available phosphorus; AK, available potassium; C genes is the absolute abundance of carbon cycling genes; N genes is the absolute abundance of nitrogen cycling genes; P genes is the absolute abundance of phosphorus cycling genes; and GWP, global warming potential. Only indicators with significant correlation are included.

increasing micropore volume may drive functional recovery more effectively than macropore connectivity.

4.2 Synergistic mechanisms for enhanced nutrient availability

From a redox perspective, continuous oxygen release significantly increased ORP, altering nutrient chemical forms and availability. First, the reducing substances were oxidized, with TRS decreasing by ~20% (Fig. 2(a)) and Fe^{2+} by >38.5% (Fig. 2(c)), which can mitigate toxicity on crops. Second, Fe^{2+} oxidation to Fe^{3+} did not increase P fixation and reduce P availability (AP doubled with O_2-MNBs). This might occur because Fe^{2+} oxidation reduced Vivianite crystallization (which fixes P)[53] and increased P solubilization and transformation genes (Fig. 5(e)). Third, improved oxidation promoted organic N mineralization. AN increased by 24.4% with O_2-MNBs, but NH_4^+-N and NO_3^--N remained stable. This may be related to N cycling genes. Despite increased O_2, ammonia oxidation genes (*amoA-1*, *amoA-2*, *amoB* and *hao*) did not increase (Fig. 5(d)), limiting NH_4^+-N oxidation. Though denitrification genes (*napA*, *narG*, *nasA*, *nirK-1*, *nirK-2*, *nirK-3*, *nirS-1*, *nirS-2*, *nirS-3*, *nosZ-1* and *nosZ-2*) increased (Fig. 5(d)) with more organic substrates, which could potentially enhance denitrification[54], the higher ORP likely suppressed it. Thus,

moderate ORP elevation by MNBs breaks nutrient locks under reduction without causing severe nitrogen loss.

Additionally, micropore optimization enhances nutrient availability via physical and biological interfaces. Increased micropores and SSA provide more sites for nutrient adsorption-desorption[55]. Micropore porosity strongly correlates with AN (r = 0.72), AP (r = 0.90) and AK (r = 0.87) (Fig. 6, P < 0.05), identifying micropores as key for nutrient retention and release. Physically, micropores extend nutrient diffusion paths[56], reducing leaching risk. Biologically, micropores provide microhabitats for microorganisms (e.g., P-solubilizing bacteria and ammonifiers)[50,51], promoting microbial nutrient transformation. Mantel tests showed stronger and more significant correlations of nutrients with pore structure (r = 0.70–0.77) than ORP (r = 0.46), emphasizing the foundational framework of physical structure optimization for nutrient availability. This synergy makes MNBs potentially superior to common chemical amendments (only altering chemistry) and engineering drainage (only optimizing macropores) in enhancing nutrient availability.

4.3 Comprehensive effects and mechanisms of greenhouse gas emissions

MNBs significantly reduced GWP mainly by reducing CH_4 emissions by 61%, which offset increased CO_2. Greenhouse gas emissions are closely linked to microbial composition and function. Although some studies found MNBs alter microbial diversity or richness[29,48,57,58], α-diversity remained unchanged here. However, microbial community shifted significantly (NMDS, P = 0.016, Fig. S6(a)). This indicates MNBs regulate microbial functions via niche differentiation rather than species richness.

Functional gene analyses reveal mechanisms of greenhouse gas emissions. O_2-MNBs significantly increased abundance of recalcitrant C (lignin and pectin) degradation genes. This indicates enhanced microbial decomposition of SOC, which explains doubled CO_2 emissions (Fig. 4(a)), while it is more like beneficial SOC turnover rather than a significant loss of soil carbon stocks. It is accompanied by increased nutrient availability, which distinguish it from general carbon loss. Actually, moderate decomposition of recalcitrant organic carbon (e.g., peaty substances) may instead enhance the activity of soil carbon pools and improve their long-term carbon sequestration potential[59]. Nevertheless, with due caution, we must acknowledge that the long-term use of MNBs might harm soil fertility or carbon sequestration, so this requires further research. Reduced CH_4 emissions, consistent with other studies[19], resulted from direct suppression of methanogen activity by high ORP (> 349 mV, Fig. S3(b))[60] and increased methane oxidation gene abundances (*mmoX*, *mxaF*, *pqq-mdh* and *pmoA*; Fig. 5(c)) that will enhance CH_4 consumption.

Contrary to expectations that improved oxidation would promote nitrification and incomplete denitrification and increase N_2O[61], MNB treatments had no significant effect on N_2O emissions. Besides the explanations invoking O_2 diffusion limitations from increased moisture, or enhanced complete nitrification and reduced denitrification[52,62], our analyses identified three other reasons. First, nitrite oxidation genes increased but ammonia oxidation genes (the rate-limiting step in nitrification) did not, and N_2O from nitrification primarily originates from ammonia oxidation[63]. Second, enriched denitrification genes (Fig. 5(d)), especially *nosZ*, indicate enhanced N_2O reduction to N_2. This is supported by more labile organic substrates from active C metabolism (Fig. 5(b)) and micropore-scale anoxic microsites[64]. Third, prolonged O_2 exposure induces a denitrification phenotype with accelerated N_2O reduction, a phenomenon noted in previous study[65].

4.4 Theoretical significance and application potential of micro-nano bubble regulation

This study highlights the importance of soil micropores. Research on paddy soil improvement mostly focuses on nutrients, chemistry and microorganisms[66–68]. Micropores are frequently overlooked. While macropores are normally thought to dominate aeration and material transport[46], we found stronger and more significant correlations of nutrient availability (AN, AP and AK) with pore structure than ORP (Fig. S8). This identifies micropores as a critical threshold for soil function. Overall, MNBs directly drive nutrient availability and ecological optimization via physical structure remodeling, while ORP indirectly affects ecology by enhancing nutrients (Fig. S9). This highlights the need to consider micropore optimization in agricultural soil improvement.

Compared to existing technologies, MNBs offer three distinct advantages in improving waterlogged low-yield paddies. (1) Using air or O_2 as raw materials, MNBs leave no chemical residues and do not alter soil pH. Risks such as soil compaction from amendments (e.g. calcium peroxide) are avoided[69,70]. (2) The vast majority of the cost for MNB treatment comes from equipment purchase (several thousand yuan), which can be amortized over the operational lifespan of the equipment.

The only ongoing cost during application is the energy consumption. Therefore, MNBs are cost-effective and can be applied via irrigation systems without large-scale engineering. (3) MNB treatments achieve multidimensional benefits: reducing reductive substance toxicity, increasing nutrient availability and lowering greenhouse gas emissions. This addresses the productivity-ecology trade-off.

5 Conclusions

This study confirms that MNBs improve waterlogged low-yield paddy soils and enhance ecological benefits simultaneously. Key improvements include micropore restructuring and increased ORP, driven by a synergy of physical, chemical and biological processes. This finding provides valuable insights into how soil microstructure, nutrients and microorganisms collectively influence soil function and ecology. As a sustainable, low-cost technology, MNB treatment shows great potential in remediating waterlogged paddies and similar soils, supporting efficient irrigation practices and global food security, while contributing to agricultural carbon neutrality goals.

Supplementary materials

The online version of this article at http://doi.org/10.15302/J-FASE-2026673 contains supplementary materials (Figs. S1–S9; Tables S1–S6).

Acknowledgements

This work was supported by the National Key Research and Development Program of China (2024YFD1700300), the National Natural Science Foundation of China (42320104002), and the Original Innovation Project of Chinese Academy of Sciences (ZDBS-LY-DQC024).

Compliance with ethics guidelines

Zhihao Chen, Shunyao Zhuang, and Yonghong Wu declare that they have no conflicts of interest or financial conflicts to disclose. This article does not contain any studies with human or animal subjects performed by any of the authors.

REFERENCES

1. Alexandratos N, Bruinsma J. World Agriculture Towards 2030/2050: The 2012 Revision. Rome: *FAO*, 2012
2. Keating B A, Herrero M, Carberry P S, Gardner J, Cole M B. Food wedges: framing the global food demand and supply challenge towards 2050. *Global Food Security*, 2014, **3**(3–4): 125–132
3. Zeng X B, Zhang J B, Wei C F, Yu W T, Huang D Y, Xu M G, Xu J M. The status and reclamation strategy of low-yield fields in China. *Acta Pedologica Sinica*, 2014, **51**(4): 675–682 (in Chinese)
4. Liu Z, Zhou W, Li S, He P, Liang G, Lv J, Jin H. Assessing soil quality of gleyed paddy soils with different productivities in subtropical China. *Catena*, 2015, **133**: 293–302
5. Wang F, Lin C, Li Q H, Lin X J, Yu G L. A review on improvement and utilization of southern cold-waterlogged paddy fields in China. *Chinese Journal of Eco-Agriculture*, 2016, **24**(9): 1151–1160 (in Chinese)
6. Yang Y, Wang Z, Xie Y, Ataie-Ashtiani B, Simmons C T, Luo Q, Chen G, Zhang Q, Wu J, Wang J, Wu J. Impacts of groundwater depth on regional scale soil gleyization under changing climate in the Poyang Lake Basin, China. *Journal of Hydrology*, 2019, **568**: 501–516
7. Hewitt A E, Balks M R, Lowe D J. Gley soils. In: Hewitt A E, Balks M R, Lowe D J, eds. The soils of Aotearoa New Zealand. Gewerbestrasse: *Springer International Publishing*, 2021, 73–85
8. Bedard-Haughn A. Gleysolic soils of Canada: genesis, distribution, and classification. *Canadian Journal of Soil Science*, 2011, **91**(5): 763–779
9. Sahrawat K L. Iron toxicity in wetland rice and the role of other nutrients. *Journal of Plant Nutrition*, 2005, **27**(8): 1471–1504
10. Marschner P. Processes in submerged soils-linking redox potential, soil organic matter turnover and plants to nutrient cycling. *Plant and Soil*, 2021, **464**(1–2): 1–12
11. Intergovernmental Panel on Climate Change (IPCC). Climate Change 2023: Synthesis Report. Contribution of Working Groups I, II and III to the Sixth Assessment Report of the

Intergovernmental Panel on Climate Change. Geneva: *IPCC*, 2023

12. Zhang W, Yu Y, Huang Y, Li T, Wang P. Modeling methane emissions from irrigated rice cultivation in China from 1960 to 2050. *Global Change Biology*, 2011, **17**(12): 3511–3523
13. Cai Z C, Tsuruta H, Minami K. Methane emission from rice fields in China: measurements and influencing factors. *Journal of Geophysical Research*, 2000, **105**(D13): 17231–17242
14. Clagnan E, Rolfe S A, Thornton S F, Krol D, Richards K G, Lanigan G, Tuohy P, Fenton O. Nitrogen transformation processes and gaseous emissions from a humic gley soil at two water filled pore spaces. *Soil & Tillage Research*, 2020, **198**: 104543
15. Zhu X, Burger M, Doane T A, Horwath W R. Ammonia oxidation pathways and nitrifier denitrification are significant sources of N_2O and NO under low oxygen availability. *Proceedings of the National Academy of Sciences of the United States of America*, 2013, **110**(16): 6328–6333
16. Kovalev I V, Semenov V M, Kovaleva N O, Lebedeva T N, Yakovleva V M, Pautova N B. Estimation of the biogenicity and bioactivity of gleyed agrogray nondrained and drained soils. *Eurasian Soil Science*, 2021, **54**(7): 1059–1067
17. Liu Z, Xiong Y, Xu J, Yang S, Jiang Z, Liu F. Optimal operation model of drainage works for minimizing waterlogging loss in paddy fields. *Water*, 2021, **13**(20): 2811
18. Pandey A K, Singh A G, Gadhiya A R, Kumar S, Singh D, Mehta R. Chapter 17—Current approaches in horticultural crops to mitigate waterlogging stress. In: Rai A C, Rai A, Rai K K, Rai V P, Kumar A, eds. Stress Tolerance in Horticultural Crops. Cambridge: *Woodhead Publishing*, 2021, 289–299
19. Minamikawa K, Makino T. Oxidation of flooded paddy soil through irrigation with water containing bulk oxygen nanobubbles. *Science of the Total Environment*, 2020, **709**: 136323
20. Cui Y F, Meng J, Wang Q X, Zhang W M, Cheng X Y, Chen W F. Effects of straw and biochar addition on soil nitrogen, carbon, and super rice yield in cold waterlogged paddy soils of North China. *Journal of Integrative Agriculture*, 2017, **16**(5): 1064–1074
21. Wang Z Y, Han Y L, Luo S, Rong X M, Song H X, Jiang N, Li C W, Yang L. Calcium peroxide alleviates the waterlogging stress of rapeseed by improving root growth status in a rice-rape rotation field. *Frontiers in Plant Science*, 2022, **13**: 1048227
22. Du X B, He W C, Wang Z, Xi M, Xu Y Z, Wu W G, Gao S Q, Liu D, Lei W X, Kong L C. Raised bed planting reduces waterlogging and increases yield in wheat following rice. *Field Crops Research*, 2021, **265**: 108119
23. Ghaani M R, Kusalik P G, English N J. Massive generation of metastable bulk nanobubbles in water by external electric fields. *Science Advances*, 2020, **6**(14): eaaz0094
24. Jia M Y, Farid M U, Kharraz J A, Kumar N M, Chopra S S, Jang A, Chew J, Khanal S K, Chen G H, An A K. Nanobubbles in water and wastewater treatment systems: small bubbles making big difference. *Water Research*, 2023, **245**: 120613
25. Marcelino K R, Ling L, Wongkiew S, Nhan H T, Surendra K C, Shitanaka T, Lu H, Khanal S K. Nanobubble technology applications in environmental and agricultural systems: opportunities and challenges. *Critical Reviews in Environmental Science and Technology*, 2023, **53**(14): 1378–1403
26. Zhou S N, Qiao L, Jia Y Y, Khanal S K, Sun L P, Lu H. Micro-nano bubble ozonation for effective treatment of ibuprofen-laden wastewater and enhanced anaerobic digestion performance. *Water Research*, 2025, **273**: 123006
27. Zhang Y Y, Cai L, Chen L H, Zhang H, Li G Q, Wang G X, Cui J, Filatova I, Liu Y N. Effect of micro-nano bubbles on the remediation of saline-alkali soil with microbial agent. *Science of the Total Environment*, 2024, **912**: 168940
28. Lei H J, Wang W B, Liang Y Q, Xiao Z Y, Pan H W, Wang L Y, Du M Y. Effect of nano-bubble irrigation on the yield and greenhouse gas warming potential of greenhouse tomatoes. *Agronomy*, 2023, **13**(12): 2917
29. Zhou Y P, Bastida F, Zhou B, Sun Y F, Gu T, Li S Q, Li Y K. Soil fertility and crop production are fostered by micro-nano bubble irrigation with associated changes in soil bacterial community. *Soil Biology & Biochemistry*, 2020, **141**: 107663
30. Yang W, Peng X D, Dai Q H, Li C L, Xu S B, Liu T T. Storage infiltration of rock-soil interface soil on rock surface flow in the rocky desertification area. *Geoderma*, 2023, **435**: 116512
31. Makeev A, Rusakov A, Lebedeva M, Karpukhina N, Konstantinov E, Frechen M, Kust P. Unveiling the enigma of the upper Volga River valley based on the soilscape studies. *Catena*, 2024, **246**: 108431
32. Wei X M, Ge T D, Wu C F, Wang S, Mason-Jones K, Li Y, Zhu Z K, Hu Y J, Liang C, Shen J L, Wu J S, Kuzyakov Y. T4-like phages reveal the potential role of viruses in soil organic matter mineralization. *Environmental Science & Technology*, 2021, **55**(9): 6440–6448
33. Yue Y, Shen C C, Ge Y. Biochar accelerates the removal of tetracyclines and their intermediates by altering soil properties. *Journal of Hazardous Materials*, 2019, **380**: 120821
34. Che W K, Piao J L, Gao Q, Li X B, Li X, Jin F. Response of soil physicochemical properties, soil nutrients, enzyme activity and rice yield to rice straw returning in highly saline-alkali paddy soils. *Journal of Soil Science and Plant Nutrition*, 2023, **23**(3): 4396–4411
35. Lv W R, Luo Y S, Song C, Zhao R Q, Zheng M L. Elucidation of effects of pore structure in dual-scale electrodes on mass transfer in VRFB via nonsolvent-induced phase separation and laser perforation. *Chemical Engineering Journal*, 2025, **507**: 160412
36. Xiao R H, Man X L, Duan B X, Cai T J, Ge Z X, Li X F, Vesala

T. Changes in soil bacterial communities and nitrogen mineralization with understory vegetation in boreal larch forests. *Soil Biology & Biochemistry*, 2022, **166**: 108572

37. Bolger A M, Lohse M, Usadel B. Trimmomatic: a flexible trimmer for Illumina sequence data. *Bioinformatics*, 2014, **30**(15): 2114–2120
38. Martin M. Cutadapt removes adapter sequences from high-throughput sequencing reads. *EMBnet.Journal*, 2011, **17**(1): 10–12
39. Bolyen E, Rideout J R, Dillon M R, Bokulich N A, Abnet C C, Al-Ghalith G A, Alexander H, Alm E J, Arumugam M, Asnicar F, Bai Y, Bisanz J E, Bittinger K, Brejnrod A, Brislawn C J, Brown C T, Callahan B J, Caraballo-Rodríguez A M, Chase J, Cope E K, Da Silva R, Diener C, Dorrestein P C, Douglas G M, Durall D M, Duvallet C, Edwardson C F, Ernst M, Estaki M, Fouquier J, Gauglitz J M, Gibbons S M, Gibson D L, Gonzalez A, Gorlick K, Guo J R, Hillmann B, Holmes S, Holste H, Huttenhower C, Huttley G A, Janssen S, Jarmusch A K, Jiang L J, Kaehler B D, Kang K B, Keefe C R, Keim P, Kelley S T, Knights D, Koester I, Kosciolek T, Kreps J, Langille M G I, Lee J, Ley R, Liu Y X, Loftfield E, Lozupone C, Maher M, Marotz C, Martin B D, McDonald D, McIver L J, Melnik A V, Metcalf J L, Morgan S C, Morton J T, Naimey A T, Navas-Molina J A, Nothias L F, Orchanian S B, Pearson T, Peoples S L, Petras D, Preuss M L, Pruesse E, Rasmussen L B, Rivers A, Robeson M S II, Rosenthal P, Segata N, Shaffer M, Shiffer A, Sinha R, Song S J, Spear J R, Swafford A D, Thompson L R, Torres P J, Trinh P, Tripathi A, Turnbaugh P J, Ul-Hasan S, van der Hooft J J J, Vargas F, Vázquez-Baeza Y, Vogtmann E, von Hippel M, Walters W, Wan Y H, Wang M X, Warren J, Weber K C, Williamson C H D, Willis A D, Xu Z Z, Zaneveld J R, Zhang Y L, Zhu Q Y, Knight R, Caporaso J G. Reproducible, interactive, scalable and extensible microbiome data science using QIIME 2. *Nature Biotechnology*, 2019, **37**(8): 852–857
40. Callahan B J, McMurdie P J, Rosen M J, Han A W, Johnson A J A, Holmes S P. DADA2: high-resolution sample inference from Illumina amplicon data. *Nature Methods*, 2016, **13**(7): 581–583
41. Quast C, Pruesse E, Yilmaz P, Gerken J, Schweer T, Yarza P, Peplies J, Glöckner F O. The SILVA ribosomal RNA gene database project: improved data processing and web-based tools. *Nucleic Acids Research*, 2013, **41**(D1): D590–D596
42. Zheng B X, Zhu Y G, Sardans J, Peñuelas J, Su J Q. QMEC: a tool for high-throughput quantitative assessment of microbial functional potential in C, N, P, and S biogeochemical cycling. *Science China. Life Sciences*, 2018, **61**(12): 1451–1462
43. Roberts D W. Distance, dissimilarity, and mean–variance ratios in ordination. *Methods in Ecology and Evolution*, 2017, **8**(11): 1398–1407
44. The Comprehensive R Archive Network (CRAN). R Package: Partial Least Squares Path Modeling (PLS-PM) version 0.6.0. 2025. Available at CRAN website on September 26, 2025
45. He D, Dai Z M, Cheng S X, Shen H J, Lin J H, Zhao K K, Rodrigues Jorge L M, Kuzyakov Y, Xu J M. Microbial life-history strategies and genomic traits between pristine and cropland soils. *mSystems*, 2025, **10**(5): e00178–25
46. Li Z, Kravchenko A N, Cupples A, Guber A K, Kuzyakov Y, Philip Robertson G, Blagodatskaya E. Composition and metabolism of microbial communities in soil pores. *Nature Communications*, 2024, **15**(1): 3578
47. Word C S, McLaughlin D L, Strahm B D, Stewart R D, Varner J M, Wurster F C, Amestoy T J, Link N T. Peatland drainage alters soil structure and water retention properties: implications for ecosystem function and management. *Hydrological Processes*, 2022, **36**(3): e14533
48. Chen W J, Bastida F, Liu Y Z, Zhou Y P, He J, Song P, Kuang N K, Li Y K. Nanobubble oxygenated increases crop production via soil structure improvement: the perspective of microbially mediated effects. *Agricultural Water Management*, 2023, **282**: 108263
49. Arablousabet Y, Povilaitis A. The impact of nanobubble gases in enhancing soil moisture, nutrient uptake efficiency and plant growth: a review. *Water*, 2024, **16**(21): 3074
50. Hartmann M, Six J. Soil structure and microbiome functions in agroecosystems. *Nature Reviews. Earth & Environment*, 2023, **4**(1): 4–18
51. Philippot L, Chenu C, Kappler A, Rillig M C, Fierer N. The interplay between microbial communities and soil properties. *Nature Reviews. Microbiology*, 2024, **22**(4): 226–239
52. Baram S, Evans J F, Berezkin A, Ben-Hur M. Irrigation with treated wastewater containing nanobubbles to aerate soils and reduce nitrous oxide emissions. *Journal of Cleaner Production*, 2021, **280**: 124509
53. Li J H, Chen H J, Bu H L, Wei Y F, Chen M Q, Xu W P, Hao X Y, Yuan P. Fe(II)-humus interactions drive phosphorus immobilization: insights into vivianite formation. *Journal of Environmental Sciences*, 2025 [in press]
54. Li Z L, Tang Z, Song Z P, Chen W N, Tian D S, Tang S M, Wang X Y, Wang J S, Liu W J, Wang Y, Li J, Jiang L F, Luo Y Q, Niu S L. Variations and controlling factors of soil denitrification rate. *Global Change Biology*, 2022, **28**(6): 2133–2145
55. Yang J, Xin X L, Zhang X F, Zhong X Y, Yang W L, Ren G C, Zhu A N. Effects of soil physical and chemical properties on phosphorus adsorption-desorption in fluvo-aquic soil under conservation tillage. *Soil & Tillage Research*, 2023, **234**: 105840
56. Gao Y R, Fang Z, Van Zwieten L, Bolan N, Dong D, Quin B F, Meng J, Li F B, Wu F C, Wang H L, Chen W F. A critical review of biochar-based nitrogen fertilizers and their effects on crop production and the environment. *Biochar*, 2022, **4**(1): 36
57. Zhou Y P, Bastida F, Liu Y Z, He J, Chen W J, Wang X Y, Xiao Y, Song P, Li Y K. Impacts and mechanisms of nanobubbles

level in drip irrigation system on soil fertility, water use efficiency and crop production: the perspective of soil microbial community. *Journal of Cleaner Production*, 2022, **333**: 130050

58. Wang J W, Cui Y Q, Wu K L, Wu S Y, Wu K J, Li Y, Niu W Q. Micro/nanobubble-aerated drip irrigation affects saline soil microenvironments and tomato growth by altering bacterial communities. *Soil & Tillage Research*, 2024, **239**: 106034
59. Zhou Y, Zhang J W, Xu L, Nadeem M Y, Li W W, Jiang Y, Ding Y F, Liu Z H, Li G H. Long-term fertilizer postponing promotes soil organic carbon sequestration in paddy soils by accelerating lignin degradation and increasing microbial necromass. *Soil Biology & Biochemistry*, 2022, **175**: 108839
60. Shi W Q, Pan G, Chen Q W, Song L R, Zhu L, Ji X N. Hypoxia remediation and methane emission manipulation using surface oxygen nanobubbles. *Environmental Science & Technology*, 2018, **52**(15): 8712–8717
61. Zhu G B, Shi H, Zhong L, He G, Wang B Z, Shan J, Han P, Liu T X, Wang S Y, Liu C L, Zhang N, Jiang L P, Yu L B, Zhan C H, Tang Z Y, Wen T, Ma B, Su X X, Zhang S J, Zhang J B, Di H J, Hou L J, Krichels A H, Trimmer M, Jetten M S M, Peng Y Z, Löffler F E, Tian H Q, Zhu Y G. Nitrous oxide sources, mechanisms and mitigation. *Nature Reviews. Earth & Environment*, 2025, **6**(9): 574–592
62. Du Y D, Gu X B, Wang J W, Niu W Q. Yield and gas exchange of greenhouse tomato at different nitrogen levels under aerated irrigation. *Science of the Total Environment*, 2019, **668**: 1156–1164
63. Wang S Y, Lan B R, Yu L B, Xiao M Y, Jiang L P, Qin Y, Jin Y C, Zhou Y T, Armanbek G, Ma J C, Wang M T, Jetten M S M, Tian H Q, Zhu G B, Zhu Y G. Ammonium-derived nitrous oxide is a global source in streams. *Nature Communications*, 2024, **15**(1): 4085
64. Borer B, Tecon R, Or D. Spatial organization of bacterial populations in response to oxygen and carbon counter-gradients in pore networks. *Nature Communications*, 2018, **9**(1): 769
65. Sennett L B, Roco C A, Lim N Y N, Yavitt J B, Dörsch P, Bakken L R, Shapleigh J P, Frostegård Å. Determining how oxygen legacy affects trajectories of soil denitrifier community dynamics and N_2O emissions. *Nature Communications*, 2024, **15**(1): 7298
66. Jiang Y, Zhou H, Gu J F, Zeng P, Liao B H, Xie Y H, Ji X H. Combined amendment improves soil health and brown rice quality in paddy soils moderately and highly co-contaminated with Cd and As. *Environmental Pollution*, 2022, **295**: 118590
67. Song W F, Shu A P, Liu J A, Shi W C, Li M C, Zhang W X, Li Z Z, Liu G R, Yuan F S, Zhang S X, Liu Z B, Gao Z. Effects of long-term fertilization with different substitution ratios of organic fertilizer on paddy soil. *Pedosphere*, 2022, **32**(4): 637–648
68. He X L, Yang Y R, Huang B S, Wang Z H, Wang M X. An overview of characteristic factors of biochar as a soil improvement tool in rice growth—A review. *Environmental Research*, 2024, **242**: 117794
69. He L Z, Xu Y, Zhang M G, Gul S, Zhang X K, Zhong H, Tang Y X, Dong D B, Xu Y, Liu D, Bolan N, Wang H L. Effect of remediation technologies on soil fertility in heavy metal(loid)-contaminated soils: a critical review. *Critical Reviews in Environmental Science and Technology*, 2024, **54**(19): 1417–1435
70. Feng H L, Cheng J M. Whole-process risk management of soil amendments for remediation of heavy metals in agricultural soil—A review. *International Journal of Environmental Research and Public Health*, 2023, **20**(3): 1869